SOME ASPECTS OF EROSIVE WAVES AT KUNDUCHI BEACH, DAR ES SALAAM, TANZANIA

Alfonse M. Dubi
Institute of Marine Sciences, University of Dar es Salaam
P.O. Box 668 Zanzibar, Tanzania
E-mail: dubi@zims.udsm.ac.tz

Abstract

The area north of the Dar es Salaam City is endowed with beautiful sandy beaches and high concentration of tourist beach hotels that are threatened by coastal erosion. In order to protect the buildings and land, coastal erosion must be controlled by mitigation options that are based on scientific data. The wave and current climate along the East African region are generally controlled by the seasonal monsoon winds. During the north-east monsoon period when winds blow from the Northeast, the wind-generated waves approach the coast from the northerly direction and produce long-shore currents with a southerly component. During the southerly monsoon period the wind direction is reversed and so is the wave and current climate. As such the erosion of the coast is expected also to be periodic in pattern and intensity.

The study area is Kunduchi Beach, which is located 10 km north of Dar es Salaam city. The beach lies on the west of the Zanzibar Channel, which separates Zanzibar from the Mainland.

Study of the near-shore waves was carried out by deploying wave gauges on the tidal flat at about 100 m from the beach and in 5 – 10 m deep water, about half a kilometre from the beach. The pressure gauges can measure up to 2.5 bar of absolute pressure. Each pressure sensor was connected to a 12-bit XR440-M data logger with a capacity of 86400 readings. Waves were recorded at a sampling frequency of 1 Hz on different dates. The data set used was recorded in April (during north-east monsoon winds) and September (during the Southeast monsoon winds). According to the measurements, the highest tide level is +2.5 m in the period of September. During low tide, the tidal flat is dry.

Results show that the deviation of the surface elevation from the Gaussian distribution does not vary very much during flooding and ebbing (std (flood) = 0.0867, std (ebbing) = 0.0954). However, it increases almost twice during high water (std (high water) = 0.14), such that the probability density function of the surface elevation becomes broad and extended.

The power spectrum at high tide is 3-peaked and is divided into three frequency regions; long waves ($f < 0.04$), swells ($0.04 < f < 0.1$) and wind waves ($f > 0.1$). During flooding and ebbing, the power spectra are broad and low-peaked, which means waves interact with the flooding and ebbing tides to induce breaking.

Significant wave height is linearly related to mean water level. It is during high water that wave activity is most intense and therefore sediment suspension is expected to be highest. It is during the south-east winds that waves are predominant for the beach processes. The highest waves arrive at the shore and break directly on the beach during high water. Since the shoreline is oriented nearly in the north-south direction and the waves reach the shoreline from the north-east during the north-east winds and reach the shore from the south-east during the southerly winds, long-shore wave induced currents will be generated. These currents will carry the suspended sediments along the shore.

1. INTRODUCTION

The coastline of Tanzania has been experiencing serious erosion and accretion in some parts. The area north of the Dar es Salaam City is endowed with beautiful sandy beaches and high concentration of tourist beach hotels that are threatened by coastal erosion. In order to protect the buildings and land, coastal erosion must be controlled by mitigation options that are based on scientific data.

The wave and current climate along the East African region are generally controlled by the

seasonal monsoon winds. During the Northeast monsoon period when winds blow from the Northeast, the wind-generated waves approach the coast from the northerly sector and produce long-shore currents with a southerly component. During the Southeast Monsoon period the wind direction is reversed and so is the wave and current climate. As such the erosion of the coast is expected also to be periodic in pattern and intensity. The coastline of Tanzania north of Dar es Salaam City is generally exposed to both winds and there is very little shelter except for isolated islets and a fringing reef. Currents and wave climate, which are very much influenced by the monsoons and the bathymetry, have not been well studied.

The study area is Kunduchi Beach, which is located 10 km north of Dar es Salaam City, Tanzania (Figures 1 and 2). The beach lies on the west of the Zanzibar Channel, which separates Zanzibar from the Mainland. The Channel has depths hardly exceeding 60 metres at the northern and southern entrances, while the mean depth of the Channel is 20 metres. Off Kunduchi Beach, there are three reef islands, Mbudya, Pangavini and Bongoyo (Figure 2), with a core of raised coral reef. The bathymetry between Kunduchi beach and Mbudya Island shows that there are two submerged channels which run almost parallel to the coastline. Given the presence of these channels and the high tidal range (> 4 m), it is likely that offshore waves will reach the beach and break directly on the beach slope.

Information on waves off Kunduchi Beach is not much. Lwiza (1987) measured waves at Kunduchi Beach at about 1 metre below datum using an 8-metre graduated wooden staff for only ten days after which the staff was stolen. Waves in other locations collected from visual observation. During the Northeast winds, he found that waves were low with an average height of 0.2 metres south of Mbezi River. The height increased northward such that at Africana Hotel, it was about 0.4 metres. Between Bahari Beach and Ras Kiromoni, waves were observed to have heights of about 1.2 metres. Near Kunduchi, at the sand spit, waves were choppy and confused such that no good data could be obtained using a graduated wave staff.

The objective of this study is to investigate short-term statistical parameters of the waves and get an insight of long-shore sediment transport at Kunduchi Beach.

2. FIELD MEASUREMENTS

Study of the near-shore waves was carried out by deploying wave gauges on the tidal flat at about 100 m from the beach and in 5 – 10 m deep water, about half a kilometre from the beach. The pressure gauges can measure up to 2.5 bar of absolute pressure. Each pressure sensor was connected to a 12-bit XR440-M data logger with a capacity of 86400 readings. Waves were recorded at a sampling frequency of 1 Hz. The data used are those recorded in April (during Northeast monsoon winds) and September (during the Southeast monsoon winds). According to the measurements, the highest tide level is +2.5 m in the period of September. During low tide, the tidal flat is dry.

3. RESULTS

3.1 Statistical Properties of the Waves

3.1.1 Distribution of the surface elevation and energy density

The sea surface elevation $\eta(x, y, t)$ of irregular waves is understood to be composed of an infinite number of regular wave trains with various frequencies, wave numbers and directions, which are superimposed on each other. It varies both in time and space and is expressed after Longuet-Higgins (1957) as:

$$\eta(x,y,t) = \sum a_n \cos[(k_n \cos\theta_n)x + (k_n \sin\theta_n)y - 2\pi f_n t + \varepsilon_n] \quad \text{.....(1)}$$

where a is the amplitude, k is the wave number, θ is the wave direction, f is the wave frequency, ε is the phase lag and the subscript n indicates the n-th component of a wave. At a fixed point in space, η is a function of t. One of the first steps in the analysis of a wave record at a single point is the examination of an instantaneous surface elevation sampled at a certain time interval. Basing on many instrumental observations of ocean and coastal waves, many investigators have concluded that the distribution of the surface elevation of waves is closely Gaussian, provided that non-linear interactions are small enough to assume that component waves are statistically

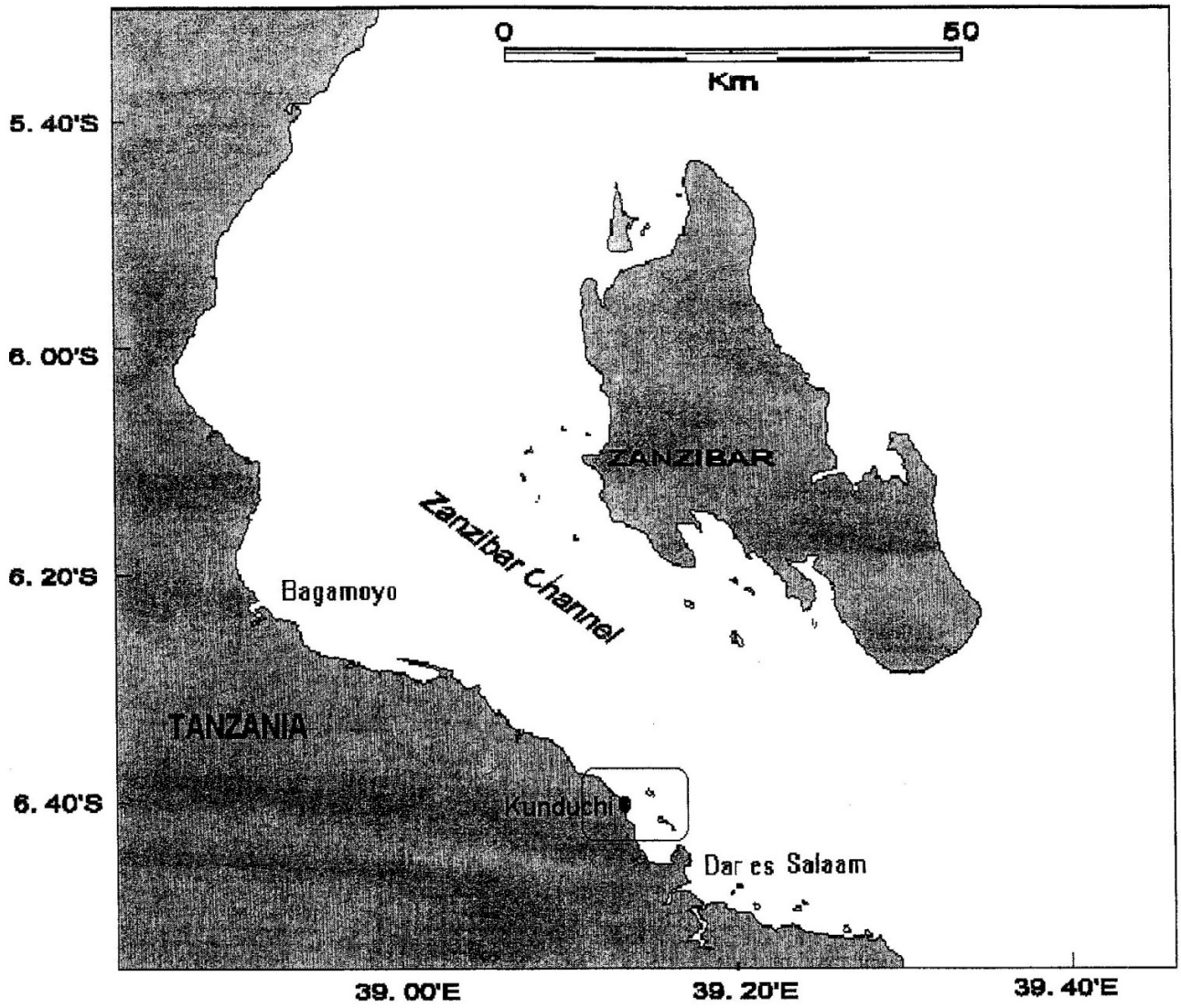

Figure 1. Location map of the study area, Kunduchi Beach, Dar es Salaam

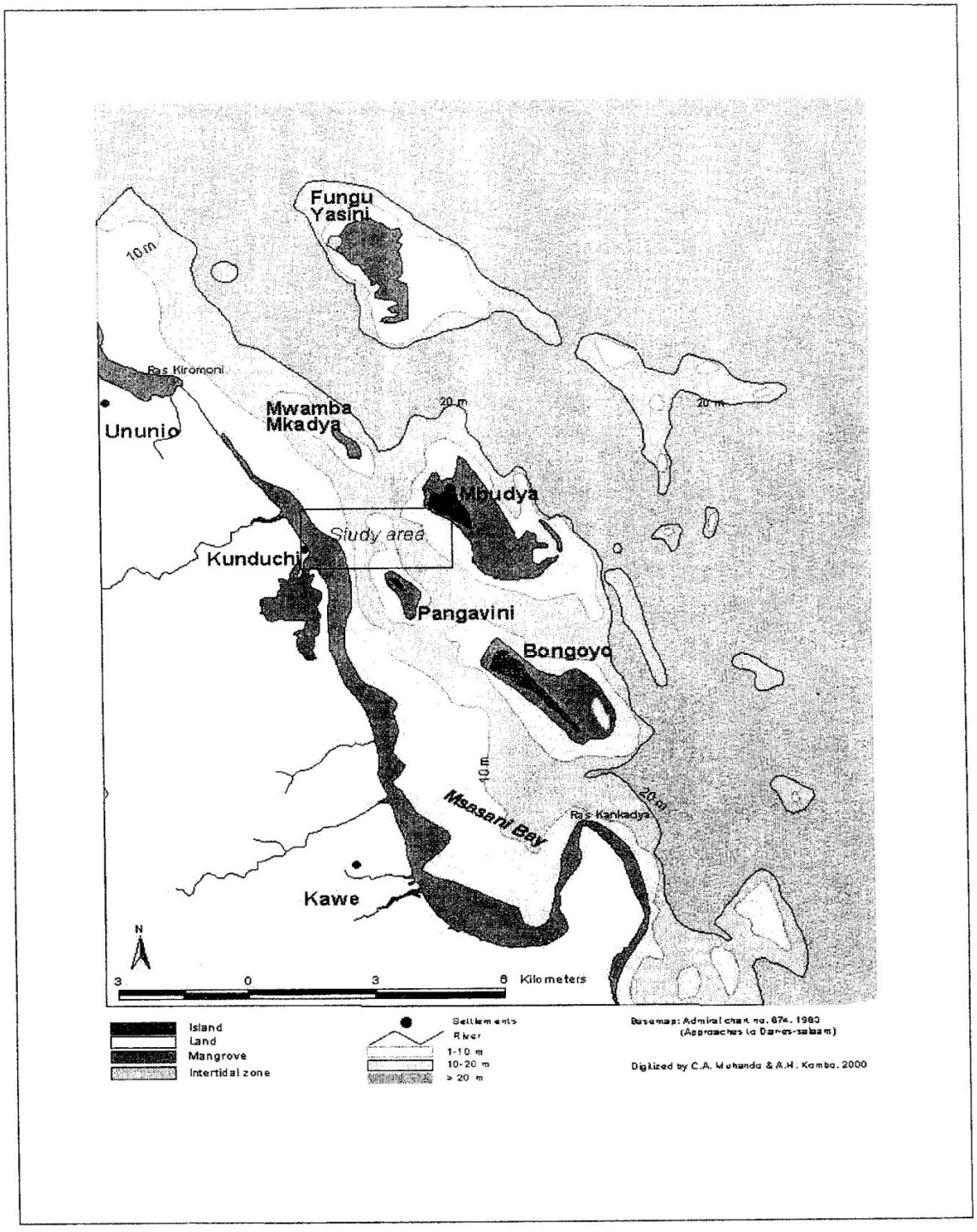

Figure 2. Physical features off Kunduchi Beach, Dar es Salaam

independent. The probability density function is given as

$$p(\eta)d\eta = \frac{1}{\sqrt{2\pi}\eta_{rms}} \exp\left[-\frac{\eta^2}{2\eta_{rms}^2}\right] \quad \text{.....(2)}$$

where η_{rms} is the root mean square value of the surface elevation η.

Statistical properties of the sea surface are described also by the energy density spectrum $S(f)$ or $S(\omega)$. The total energy density $S(f)$ is related to the total energy of a component wave whose frequency lies between f and $f + \Delta f$ as:

$$S(f)\Delta f = \sum_{f}^{f+\Delta f} \frac{1}{2} a_n^{\,2} \quad \text{.....(3)}$$

The *n-th* order of moment of an energy density spectrum is given as:

$$m_n = \int_0^\infty f^n S(f) df \quad \text{.....(4)}$$

For $n = 0$, m_0 represents the area under the energy density spectrum and is equal to one half amplitude squared.

Figure 3 shows a part of the time series of water level and wave height measured by a pressure sensor on the tidal flat 100 m from the eroding beach of Kunduchi. Figure 4 shows the probability density function of the surface elevation during flooding, high water and ebbing tide. The figure shows that during flooding and ebbing tide, the probability density function of the surface elevation are more peaked and less extended than during high water. Figure 5 shows an example of wave spectra recorded during the month of April, when the monsoon winds are north-easterly. In this figure, we see that there are mainly two groups of waves reaching the eroding beach. The main group has a spectral peak at frequency *fps* = 0.0837 Hz and the secondary group is found at the frequency twice the main spectral peak at *fpw* = 0.1674 Hz. Figure 6 shows typical wave spectra measured during September, when the winds are south-easterly. There is practically no energy in the higher and lower parts of the spectrum. The figure shows also that during the northeasterly winds, the spectra exhibit almost the same shape in a day. Waves reaching the beach can be divided into two main groups; the first group is swells (0.04< frequency < 0.1) and the second group is wind waves (frequency > 0.1).

In Figure 6, we see that during the southeasterly winds, wave spectra are generally multi-peaked and broad-banded. At high water, waves can be divided into three groups; long waves with frequency less 0.04, swells with frequencies between 0.04 and 0.1; and wind waves with frequencies greater than 0.1 Hz. Most of the energy is concentrated in swells and wind waves. Wave spectra during flooding and ebb tide are low and spread across all frequencies.

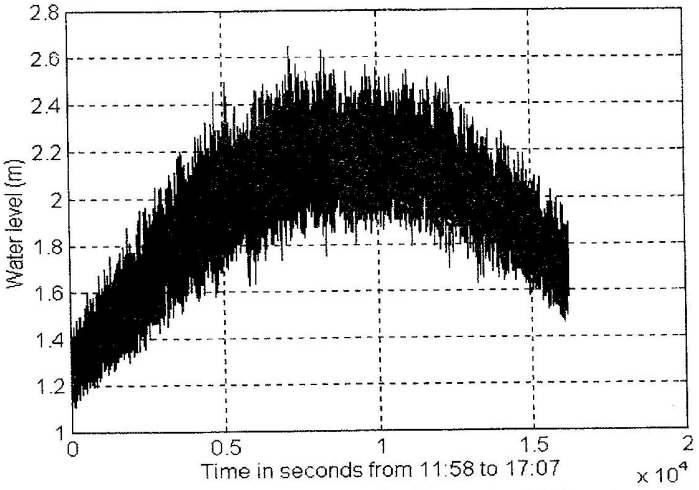

Figure 3. Time series of wave height and water level off Kunduchi Beach on 22 September 1999

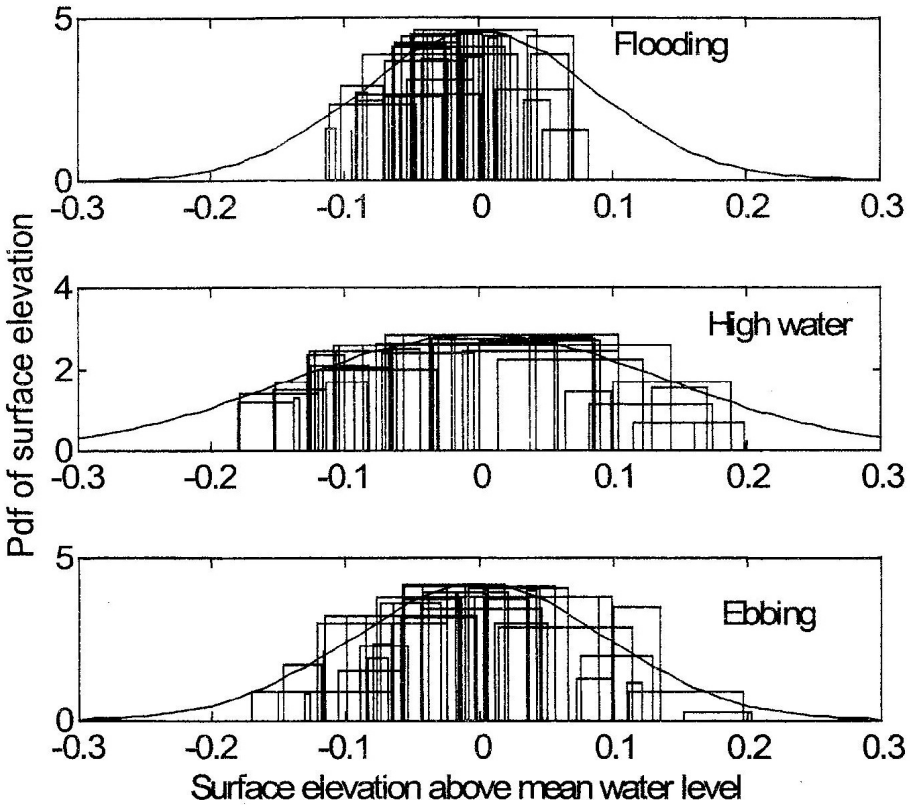

Figure 4. Observed probability density distributions of surface elevation during flooding tide, high water and ebbing tide off Kunduchi Beach. Thin solid line is the Gaussian distribution.

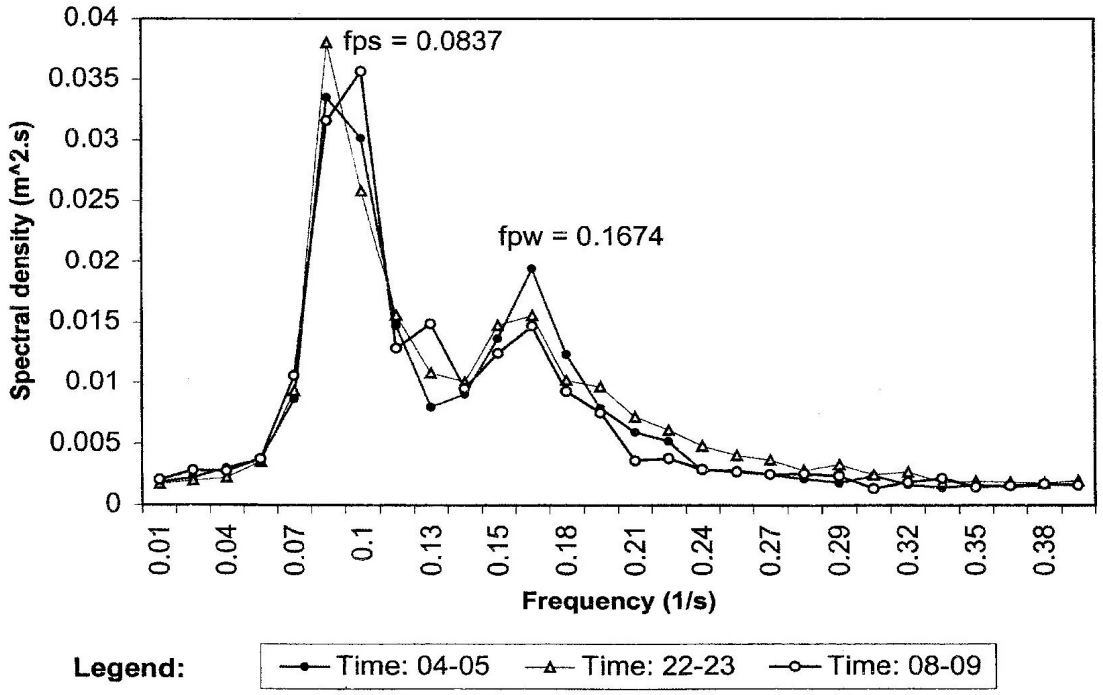

Figure 5. Typical wave spectra off Kunduchi Beach during north-east monsoon winds (*fps* is the peak frequency for swells and *fpw* is the peak frequency for wind waves.)

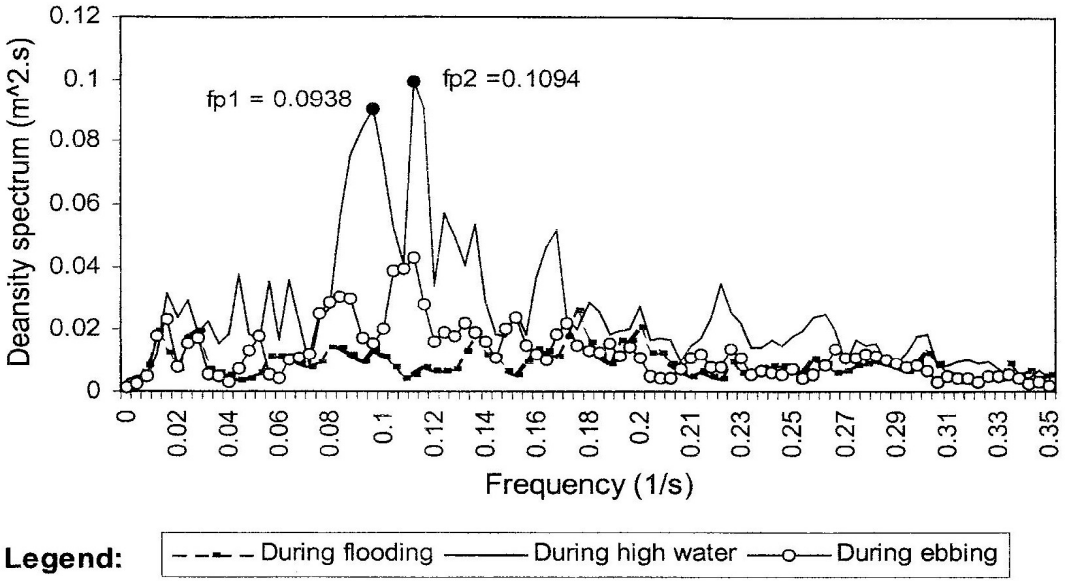

Figure 6. Typical wave spectra off Kunduchi Beach during south-east monsoon winds (*fp1,2* are peak frequencies)

3.1.2 Distribution of wave heights

Wave height distribution is an important and useful statistical description of irregular waves. For waves composed of very narrowly spread frequencies (also known as Gaussian sea state) in finite depth of water, the Rayleigh distribution is accepted as a reliable measure of the wave height distribution (Longuet-Higgins, 1952). However, as waves approach depth-limiting breaking; or as they interact nonlinearly with currents or other waves, the wave heights deviate from the Rayleigh distribution. In this case, according to Hughes and Borgman (1987), the Beta-Rayleigh distribution is a better probability distribution function and is given as:

$$p_{BR}(H)=\frac{2\Gamma(\alpha+\beta)}{\Gamma(\alpha)\Gamma(\beta)}\frac{H^{2\alpha-1}}{H_b^{2\alpha}}\left(1-\frac{H^2}{H_b^2}\right)^{\beta-1} \qquad (5)$$

valid in the range $0 < H < H_b$, where H_b is the breaking wave height, α and β are coefficients related to the root-mean- square wave height by the expressions

$$\alpha=\frac{K_1(K_2-K_1)}{K_1^2-K_2} \quad \text{and}$$

$$\alpha=\frac{(1-K_1)_1(K_2-K_1)}{K_1^2-K_2} \qquad \ldots.(6)$$

where

$$K_1=\frac{H_{rms}^2}{H_b^2}\ ; \quad K_2=\frac{H_{rmq}}{H_b^4} \quad \text{and}$$

$$H_{rmq}=\sqrt{2}H_{rms}^2 \qquad \ldots\ldots\ldots\ldots(7)$$

Figure 7 shows the variation of energy-based significant wave height (*Hmo*) and peak period (*Tp*) with mean water level at the tidal flat off Kunduchi Beach during September. This figure shows that *Hmo* is directly related to the mean water level. The peak period, however, shows a slightly different trend. It increases with water level until high water, where it does not show a decreasing trend with decreasing water level. Figures 8 and 9 show a linear relationship of *Hmo* and *Tp* with water level. Figure 10 shows that *Hmo* is linearly related to peak period. Figure 11 shows that during high water the wave height distribution has a tendency to skew toward the high wave side of the Beta-Rayleigh distribution. Other statistically based wave height parameters such as the root-mean square wave height (*Hrms*), expected values of the mean heights of the highest one-tenth ($H_{1/10}$) and one-hundredth ($H_{1/100}$), are shown in Table 1.

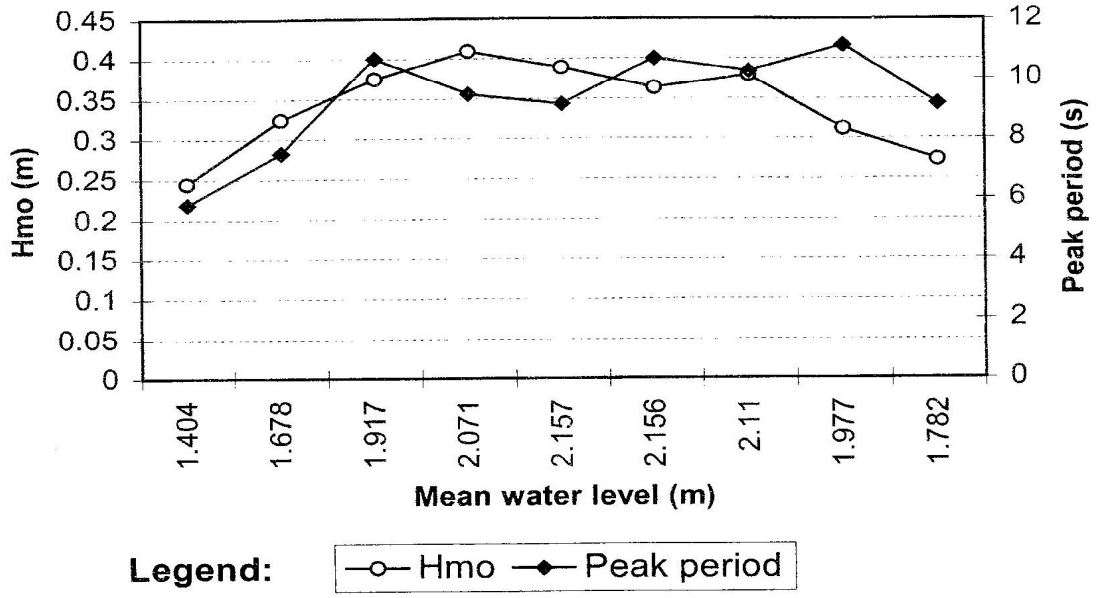

Figure 7. Variation of significant wave height and peak period with mean water level at the tidal flat off Kunduchi Beach on 22 September, 1999, from 11:58 to 17:07 hours.

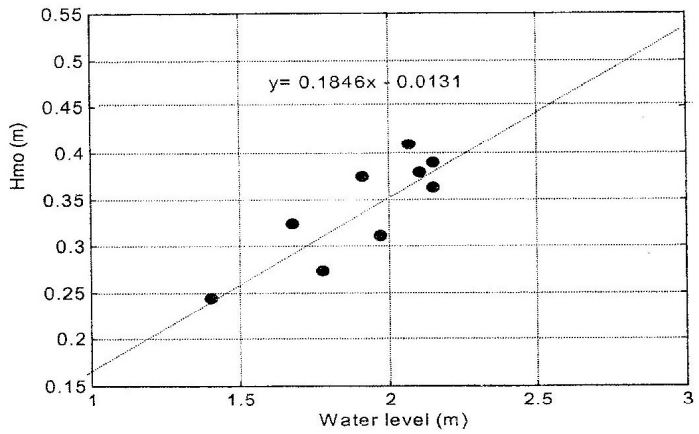

Figure 8. Relation of significant wave height with mean water level at the tidal flat off Kunduchi Beach on 22 September 1999, 30 minute records from 11.58 to 17.07 hours.

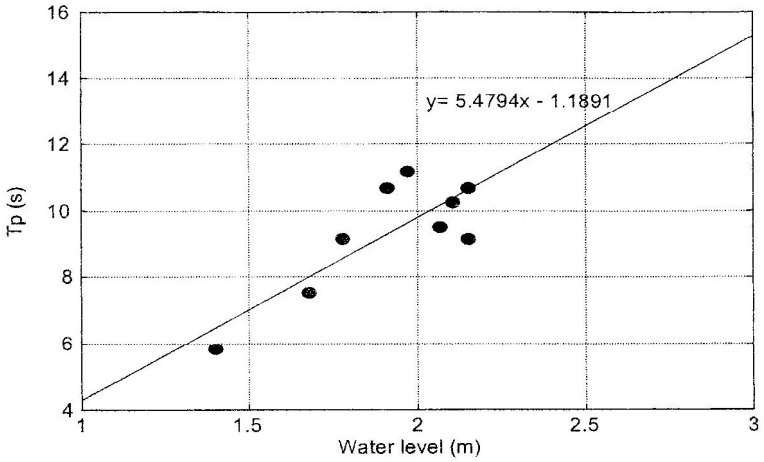

Figure 9. Relation of peak period with mean water level at the tidal flat off Kunduchi Beach on 22 September 1999, 30 minute records from 11.58 to 17.07 hours.

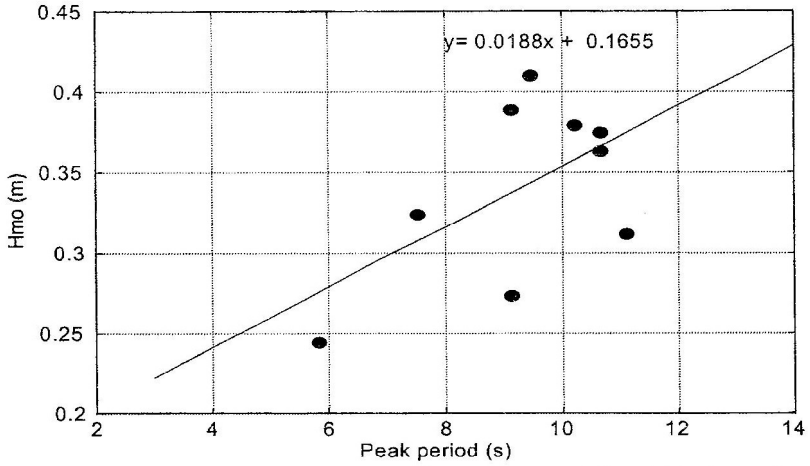

Figure 10. Relation of significant wave height with peak period the tidal flat off Kunduchi Beach on 22 September 1999, 30 minute records from 11:58 to 17:07 hours.

Table 1. Some statistical parameters of waves near Kunduchi beach

Mean water depth (m)	*Std of surface elevation (m)*	*Tp (s)*	*Hmo (m)*	*Hrms (m)*	*H(1/3) (m)*	*H(1/10) (m)*	*H(1/100) (m)*
1.40	0.0867	5.82	0.24	0.18	0.26	0.34	0.54
1.68	0.1153 0.1375	7.53	0.32	0.25	0.36	0.50	0.69
1.92	0.1411	10.67	0.37	0.31	0.46	0.52	0.61
2.07	0.1383	9.48	0.41	0.33	0.47	0.54	0.69
2.16	0.1303	9.1	0.39	0.31	0.46	0.63	0.73
2.16	0.1334	10.7	0.36	0.30	0.42	0.49	0.61
2.11	0.1109	10.24	0.38	0.31	0.43	0.54	0.82
1.98	0.0954	11.13	0.31	0.27	0.39	0.44	0.75
1.78		9.14	0.27	0.22	0.34	0.38	0.60

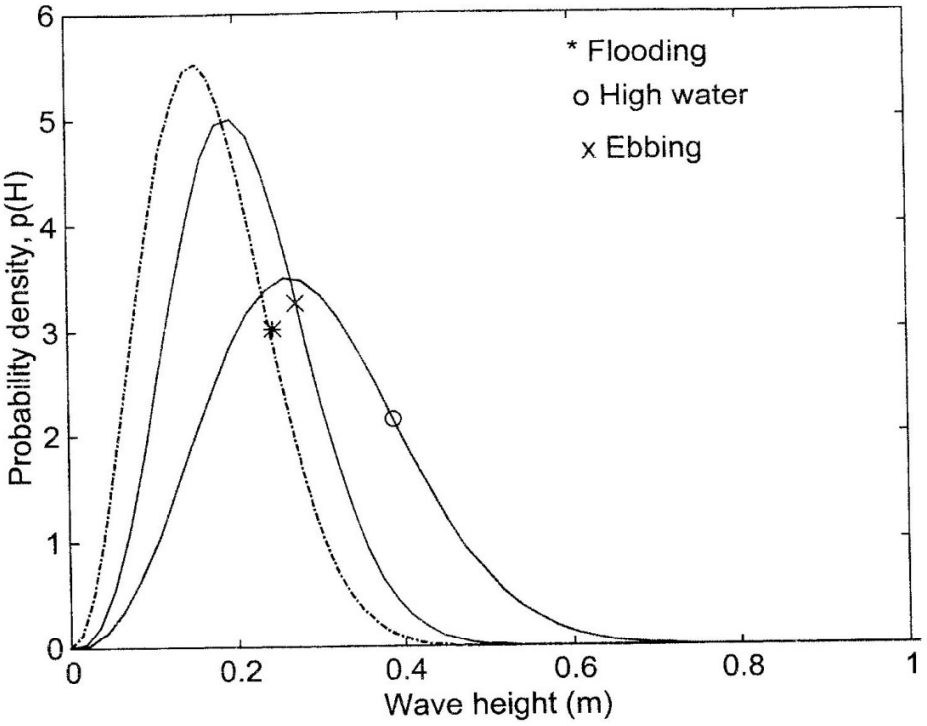

Figure 11. Beta - Rayleigh distribution of wave heights during flooding, high water and ebbing tide at Kunduchi Beach.

3.2 Long-shore sediment transport

When waves break at an appreciable angle to the shoreline, a current is created that will flow parallel to the shoreline and is confined largely to the near-shore zone between the breakers and the shoreline.

This current will carry sediments if their speed reach the threshold speed at which the sediment on the seabed begins to move. If the quantity of sediment carried away by such currents exceeds the amount naturally supplied to the beach, erosion will occur. The mean current due to oblique waves can be estimated (Komar, 1979) as:

$$\overline{v_l} = 1.17\sqrt{gH_b}\,\sin\alpha_b\cos\alpha_b \quad \text{.....(8)}$$

where v is the long-shore current at the mid-surf position, half way between the breaker zone and the shoreline, H_b is the breaker wave height, α_b is the breaker angle.

The volumetric rate of movement of sand parallel to shoreline depends on the long-shore component of wave energy flux entering the surf zone and the immersed weight of sand moved. The long-shore transport rate can be estimated using Equation 4-49 of the *Shore Protection Manual* (CERC, 1984) as:

$$Q = \frac{K}{(\rho_s - \rho)ga'} P_{ls} \quad \textit{(unit volume per second)} \ldots\ldots (9)$$

where $K = 0.39$ is the dimensionless empirical coefficient derived from field measurements ρ_s = density of sand, ρ = density of water, g = acceleration due to gravity and $a' = 0.6$ is the ratio of the volume of solids to the total volume, accounting for sand porosity and P_{ls} = long-shore component of the wave energy flux.

The energy flux per unit length of wave crest or, equivalently, the rate at which wave energy is transmitted across a plane of unit width perpendicular to the direction of wave advance is

$$P = E\,C_g \quad \text{.....(10)}$$

Where

$$E = \frac{\rho g H^2}{8} \quad \text{.....(11)}$$

is the wave energy density, in which ρ is the density of water, g is the acceleration due to gravity and H is the wave height. If the wave crests make an angle α with the shoreline, the energy flux in the direction of wave advance *per unit length of beach* is:

$$P\cos\alpha = \frac{\rho g H^2}{8} C_g \cos\alpha \quad \text{.....(12)}$$

The long-shore component of wave energy flux is therefore

$$P_l = P\cos\alpha\sin\alpha = \frac{\rho g H^2}{8} C_g \cos\alpha\sin\alpha = \frac{\rho g H^2}{16} C_g \sin 2\alpha \quad (13)$$

The assumed relation between the long-shore transport and the energy flux in the surf zone must be evaluated at the breaker line. If H_{sb} and α_b denote the breaker values of the wave characteristics (significant wave height and angle of approach), the energy flux equation (Eq. 13) for breaking wave conditions becomes

$$P_{ls} = \frac{\rho g}{16} H_{sb}^2 C_{gb} \sin 2\alpha_b \quad \text{.....(14)}$$

where $C_{gb} = n\,C_b$ and $n \approx 1.0$ in shallow water, C_b = wave phase speed at breaking. Group velocity equals wave speed at breaking and the breaking speed is given by solitary wave theory to the approximation (Galvin, 1967)

$$C_{gb} = C_b = \sqrt{2gH_b} \quad \text{.....(15)}$$

Substituting Equation 15 into Equation 14 yields the long-shore energy flux factor for breaking wave conditions (Equation 4-44 of SPM, CERC (1984)) as:

$$P_{ls} = 0.0884\rho g^{3/2} H_{sb}^{5/2} \sin 2\alpha_b \quad \text{.....(16)}$$

The breaking wave height can be estimated according to Larson and Kraus (1989a) as:

$$H_b = 0.53 H_0 \left(\frac{H_0}{L_0}\right)^{-0.24} \quad \text{.....(17)}$$

where H_0 is the deepwater wave height and L_0 is the deep water wave length estimated by

$$L_0 = \frac{g}{2\pi} T^2 \quad \text{.....(18)}$$

in which T is the wave period.

The general orientation of the shoreline of Kunduchi Beach is 330 degrees and the tidal flat is characterised by ripples. During September, waves generally approach the shore from the south-east and hence the wave crests make an angle of 75° with the shoreline. Using equations 9 to 18, the long-shore sediment transport is estimated and shown in Table 2

Table 2. Estimated long-shore sediment transport rate during September at Kunduchi beach.

Mean water depth (m)	*Tp (s)*	*Hmo (m)*	*H_b (m)*	*P_b (W/m)*	*Q (m^3/s)*
1.40	5.82	0.24	0.4935	238.1	0.0097
1.68	7.53	0.32	0.7151	602.0	0.0246
1.92	10.67	0.37	1.0184	1457.0	0.0595
2.07	9.48	0.41	0.9781	1317.0	0.0538
2.16	9.1	0.39	0.9435	1203.7	0.0491
2.16	10.7	0.36	0.9517	1229.9	0.0502
2.11	10.24	0.38	0.9486	1220.1	0.0498
1.98	11.13	0.31	0.9167	1120.1	0.0457
1.78	9.14	0.27	0.7514	681.4	0.0278

4. CONCLUSION

The deviation of the surface elevation from the Gaussian distribution does not vary very much during flooding and ebbing (std (flood) = 0.0867, std (ebbing) = 0.0954). However, it increases almost twice during high water (std (high water) = 0.14), such that the probability density function of the surface elevation becomes broad and extended as shown in Figure 4. The increase in standard deviation means waves become more non-linear due to various factors such as wave breaking and interaction of waves with the wave-generated currents.

The power spectrum at high tide is 3-peaked and is divided into three frequency regions; long waves ($f < 0.04$), swells ($0.04 < f < 0.1$) and wind waves ($f > 0.1$). During flooding and ebbing, the power spectra are broad and low-peaked, which means waves interact with the flooding and ebbing tides to induce breaking. Due to depth limitation, it is only during high tide that long-period waves and swells can reach the beach.

It is during high water that wave activity is most intense and therefore sediment suspension is expected to be highest. It is during the south-easterly winds that waves are predominant for the beach processes. The highest waves arrive at the shore and break directly on the beach during high water inducing currents that will flow along the shoreline. During the southerly monsoons, the waves approach the shore from the south-east, inducing northerly long-shore currents, which will carry suspended sediment.

5. REFERENCES

[1] Galvin, C.J. (1967). "Longshore current velocity: A review of theory and data", Reviews of Geophysics, Vol.5, No.3.

[2] Hughes, S.A. and Borgman, L.E., "Beta-Rayleigh Distribution for Shallow Water Wave Heights", *Proceedings of the American Society of Civil Engineers Specialty Conference on Coastal Hydrodynamics,* American Society of Civil Engineers, 1987, pp. 17-31.

[3] Larson, M and Kraus, N. C. (1989a). "SBEACH: Numerical Model for Simulating Storm-Induced Beach Change, Report 1: Theory and Model Foundation, Technical Report CERC-89-9, US Army Engineer Waterways Experiment Station, Coastal Engineering Research Center, Vicksburg, MS.

[4] Longuet-Higgins, M.S., " On the Statistical Distribution of Wave Heights of Sea Waves", *Journal of Marine Research,* Vol. 11, No. 3, 1952, pp. 245-266

[5] Longuet-Higgins, M.S., "The Statistical Analysis of a Random, Moving Surface", *Phil. Trans. Roy. Soc. London,* Ser. A (966), 1957, pp. 321-387

[6] Lwiza, K.M., Waves, tides, current and wind. In Beach Erosion along Kunduchi, North of Dar es Salaam. *Chapter 3. Report for National Environment Management Council by Beach Erosion Monitoring Committee*, 1987, pp. 19-25.

[7] Shore Protection manual I&II (1984), US Army Corps of Engineers (1984)., CERC, Viksburg.